The Role of Islands in Sea Ice Transport Through Nares Strait

Brandon P. Montemuro[1*] and Georgy E. Manucharyan[1]

[1]School of Oceanography, University of Washington, Seattle, WA, USA.

*Corresponding author(s). E-mail(s): bpm5026@uw.edu;
Contributing authors: gmanuch@uw.edu;

Abstract

This paper is a non-peer reviewed preprint and has been submitted for publication to JGR Oceans for peer review. Subsequent versions of this manuscript may have slightly different content.

Keywords: Sea Ice, Nares Strait, Discrete Element Model

Abstract

Nares Strait is an important export pathway of sea ice, where its transport is highly intermittent due to the formation and collapse of sea ice arches. The islands in the strait, especially Hans Island, contribute to heightened collision forces between distinct ice floes and the land. However, since even state-of-the-art climate models remain relatively coarse and use continuous sea ice rheology, the complexities of floe-scale sea ice interactions with small islands in the Nares Strait have not been sufficiently explored. Here, we use a novel discrete element model, SubZero, to identify the role of small islands in affecting intense summer-time sea ice transport in the Nares Strait. We show that SubZero can reproduce crucial sea ice characteristics, including observed area transport, intermittency of area fluxes, and floe size distribution (FSD) derived from satellite imagery. We find that the intermittency of sea ice fluxes is sensitive to the power-law exponent of the simulated FSD, and matching it to observations implies that the floe strength for fracturing must be inversely proportional to the square root of its length scale. Conducting sensitivity simulations with modified coastlines, we identified several islands as crucial pinning points that suppress sea ice transport and cause jamming, especially during low- to moderate-wind conditions. The momentum budget reveals the islands slow down sea ice through direct normal contact with colliding floes and by increasing tangential drag forces from lateral coastal boundaries. Our study emphasizes floe-scale interactions with islands and other coastlines in large-scale sea ice transport through narrow straits.

1 Introduction

The loss of Arctic sea ice is a significant concern due to its effect on the global climate [1–4]. Over ten percent of the total Arctic sea ice volume is exported annually into the Atlantic Ocean through various pathways, including Fram and Nares/Davis straits [5]. Understanding the dynamics of sea ice transport through straits is crucial for predicting the future loss of Arctic sea ice [6]. This study focuses on sea ice dynamics in Nares Strait, which is the second largest ice export pathway that connects the Arctic Ocean and the Labrador Sea [7], located between Greenland and the Canadian Archipelago (Figure 1a). The sea ice and freshwater transported via Nares Strait can have global implications as they affect deep water mass production in the Labrador Sea [8]. For example, the extensive upper layer freshening from extreme Arctic sea ice melt in 2023 may have been the cause of the deep convection shutdown [9]. With continuing global warming and weakening of sea ice in the Arctic Ocean, the sea ice export through Nares Strait has nearly tripled [6]. Despite its importance, modeling sea ice motion in Nares Strait is particularly challenging because of the pertinence of the granular behavior of sea ice, including floe fractures [10–12] and jamming [13–16], as well as the unpredictable formation and collapse of sea ice arches [15–18] (also called bridges) that lead to highly intermittent sea ice transport [19–22].

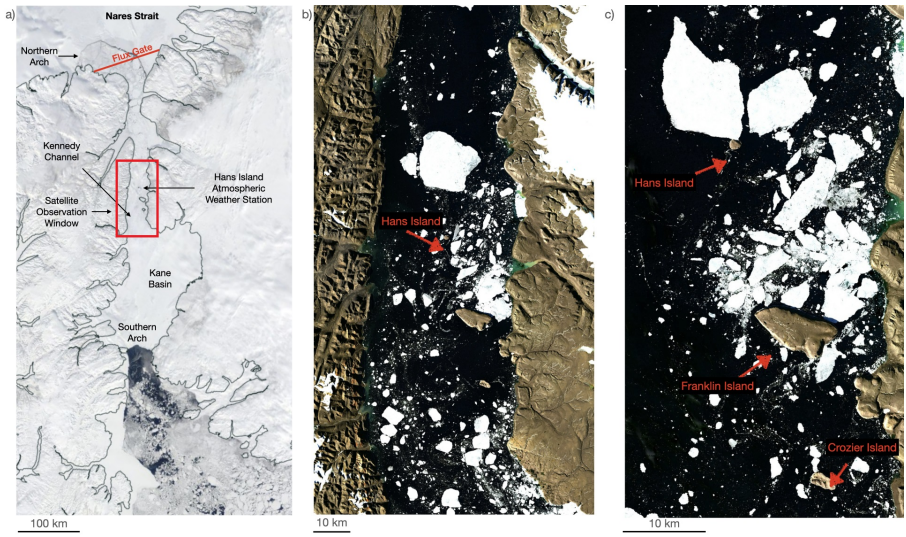

Fig. 1: Surface reflectance images of the Nares Strait. a) The Nares Strait showing conditions with both upper and lower sea ice arches formed (image taken from NASA Worldview 2023-05-04). Indicated are the locations of the Lincoln Sea flux gates (red line), the Hans Island atmospheric weather station, and the satellite observation window used to identify the floe size distributions (red rectangle). (b, c) Sea ice conditions after the breakup of arches as observed from Landsat-8 imagery on 2016-07-14 and 2016-07-16, respectively. Note the three major islands present in the Kennedy Channel section of Nares Strait. These visual observations of sea ice demonstrate large ice floes hitting Hans Island and fracturing into smaller pieces, some of which are then trapped by Franklin Island and temporarily kept from propagating through the channel.

Sea ice propagation through Nares Strait is further complicated by the presence of small islands [23], ranging from about 1 to 30 km^2 in area (Figure 1). Despite their relatively small size (e.g., Hans Island is only about 1.3 km^2), sea ice frequently comes in contact with these islands, experiencing significant collision forces [24, 25] that can result in dramatic floe fractures commonly observable from space (Figure 1c). However, the floe-scale sea ice interactions with islands and how they contribute to large-scale ice transport are poorly understood. On the one hand, islands could act as pinning points that temporarily prevent sea ice propagation. On the other hand, collisions with islands may significantly reduce floe sizes, which would result in smoother propagation of sea ice because granular media with smaller grains is known to be less prone to jamming [13]. Granular systems can jam when the forces holding them together are stronger than the forces trying to move them, such as when they are flowing through a narrow strait resulting in nearly zero motion [26, 27]. Observations in different regions of the Arctic Ocean demonstrated

that floe size distribution (FSD) of fragmented sea ice can be closely characterized by a power-law distribution, with exponents ranging roughly from -3 to -1 depending on the region, season, and floe segmentation methodology [28–34]. In contrast, in wave-affected marginal ice zones, some studies observe FSDs significantly deviating from a power law [**?**].

Climate models use continuous rheology [35], typically the elastic-viscous-plastic rheology [36] that does not explicitly simulate or take into account FSD in sea ice dynamics. These models are also very coarse and do not capture small islands, making it difficult to accurately represent the sea ice transport through Nares Strait, which is only a few tens of kilometers wide at its narrowest point in the Kennedy Channel. Regional modeling studies explored aspects of sea ice motion in Nares Strait in both continuous and discrete element models (DEMs). The formation of arches has been simulated using a continuous Maxwell elasto-brittle rheology [37] as well as with an elastic-viscous-plastic rheology [38], demonstrating the importance of arches (or bridges) in shutting down sea ice transport. However, such continuous models cannot be used to quantify the role of individual islands in the intermittent jamming behavior associated with propagation and fractures of clusters of floes. Sea ice DEMs were used to investigate jamming behavior in highly idealized constrictions [13], to explore the initial breakup events in complex coastal regions [39–41], and breakup up events with lead formation in parts of the Nares Strait [42].

However, the role of islands in the sporadic jamming, floe fractures, and propagation of sea ice through Nares Strait remains to be understood such that these processes could be parameterized in coarse-scale climate projection models. To address this issue, this study uses a unique sea ice DEM approach to explore the propagation of sea ice floes through Nares Strait shortly after the collapse of an arch, revealing the crucial role of floe collisions with small islands and coastal boundaries.

2 Methods

To simulate the propagation of sea ice in a domain with realistic coastlines and forcing, we used a sea ice DEM, SubZero [43, 44], that represents ice floes as polygons that can change shapes and fracture into smaller floes in response to stresses from collisions and external forces. SubZero is an innovative discrete element sea ice model designed to simulate the life cycles of individual ice floes using polygonal elements with dynamic boundaries. This model offers a more realistic representation of sea ice behavior at the floe scale, serving as an alternative to traditional continuous rheology models and existing sea ice discrete element models. It incorporates detailed parameterizations of various floe-scale processes, such as collisions, rafting, ridging, fracturing, and welding, to simulate the response of ice floes to mechanical and thermodynamic forces within confined or periodic environments. These processes often result in complex floe shapes. SubZero enables the investigation of a wide array of floe interaction rules and fracture criteria, deepening our understanding of sea

ice mechanics, including variations in floe sizes and shapes. To prevent a surge in the number of floes within a model, it is essential to include only adequately large floes while classifying those below a specified minimum area as unresolved and consequently removing them from the model. Unlike many existing models that rely on predefined simple shapes, SubZero employs concave polygonal elements that evolve in complexity according to specified floe-scale processes. This ability may enhance the validation of models against empirical floe-scale observations and contribute to our understanding of sea ice physics through focused process studies. This paper employs SubZero in the Nares Strait to explore the mechanisms leading to floe fracturing and emerging FSD, as well as jamming upon interactions with islands and other coastlines, and how those affect the overall sea ice transport through the strait shortly after arch collapses. We hence limit the physical processes simulated in the model to collisions and floe fracturing, making a simplifying assumption that ridging, rafting, thermodynamic, and wave-induced fractures play a secondary role.

In the first experiment, the sea ice is initialized with the observed concentration field and forced using observational winds recorded at the Hans Island atmospheric weather station (AWS) [45, 46]. The installation of the Hans Island AWS was carried out collaboratively by a team comprising members from the United States, Canada, Denmark, and the United Kingdom in May 2008. Wind speed and direction data were made available beginning in September 2014 at 30-minute intervals through October 8, 2020, with some gaps in the data. From 2016 to 2019, we have sea ice flux data [47]. Given the availability of overlapping data sets, we specifically focused on simulating the period from May 10, 2017, to May 20, 2017, when a sea ice arch collapsed. Using these observations, we tuned the SubZero model to adequately simulate the observed FSD and area transport characteristics (see Sections 3.1 and 3.2). Following this, we conduct simulations with and without the islands and emphasize small islands' crucial role in affecting overall transport (see Sections 3.3) in the Nares Strait post a southern arch collapse.

2.1 Sensitivity Tests

For our sensitivity studies, we randomly initiated the model with floes of approximately 2-3 times the maximum size observed in the region from the images used in the analysis from section 2.3. While most sensitivity studies focused on floes with a uniform thickness of 0.5 m, one particular study investigated how different thicknesses (using floes of three distinct heights) affected model outputs. To represent the inflow of ice from the Arctic Ocean, additional floes were initialized north of the strait entrance (not shown in the figures), moving in and pushing through the strait as the simulation progresses. When this northern model domain with additional floes becomes empty, it is repopulated with new sea ice to keep a continuous supply entering the Nares Strait during these simulations. Floes are removed from the simulation once they have hit the bottom boundary of the simulation domain through the strait or drop below the designated minimum floe size. The same initial floe states were

used for all ocean sensitivity tests and minimum floe size sensitivity tests. A list of all sensitivity tests that were run is included in Supplementary Table 1. We used coastline coordinates, including islands, to create a set of coastal boundaries, which are represented in the model as indestructible static floes. The initial floe state and domain are shown in Supplementary Figure 1. Table 1 lists all other parameters set for this run.

Since the fragmentation process plays a role in determining the FSD of brittle materials [48], finding a suitable floe fracture criterion is crucial for simulating the observed FSD. In this study, we use two modifications to the default method of evaluating floe fracture criteria manucharyan2022subzero. First, we have updated the model to use a weighted mean definition of the effective homogenized floe stress that is used in the evaluation of the floe fracture criteria. Specifically, we are using an exponential decay approach to calculate the new average, as shown below:

$$\frac{d\sigma}{dt} = -\frac{1}{\tau}\left(\sigma - \sigma(t)\right), \tag{1}$$

where τ is a time scale that controls the extent to which past stresses can affect the effective stress used in fracture criteria. This new calculation emphasizes the current value of the stress with much more weight compared to past values and has the added benefit of reducing the space required in data structures. We no longer need to store the N previous stresses, where N is the number of prior time steps being averaged over. The second modification concerns the floe fracture rules. We still define a failure envelope with boundaries in the principal stress space of the floe following an elliptical yield curve, mimicking continuous viscous-plastic rheology [49]. The ice strength parameter P^* defines the scale of the failure envelope, with floes breaking into multiple pieces when their principal stresses reach or exceed the envelope boundaries. This default criterion assumes the strength to be constant for all floes ($P^* = P_0^*$). However, in this study, we introduce a scale-dependent fracture criterion that links the maximum effective stress a floe can experience to its length scale, making larger floes significantly weaker than smaller floes. Since floes are composed of ice chunks that are repeatedly fracturing, ridging, and freezing back together, they contain a high number of sharp heterogeneities that can localize stress and make those floes more fragile than their constituents. Smaller ice floes that have just emerged from fractures of larger ice floes are hypothesized to be relatively stronger. We model this by scaling the ice strength parameter with the floe size as $P^* = P_0^* \, (l/l_0)^{-\frac{1}{2}}$, where l is a floe length scale defined as the square root of its area and l_0 is a reference length scale that we choose to correspond to the minimum resolved floe size (see Table 1). While we have experimented with various power-law exponents in the scaling law, we found that the square root worked best to reproduce the observed FSD. A similar scaling law was previously proposed to reconcile differences in strength between laboratory-grown and natural sea ice, arguing that cohesion strongly decreases with increasing spatial scale because of the key role of stress concentrators in fault initiation [11].

Table 1: A list of key parameters used in the SubZero model Nares Strait simulation, including their default numerical values, a brief description, and the processes that use these parameters.

Parameter	Description	Process
$E = 5 \times 10^7$ Pa	Young's Modulus	Floe Interactions
$G = \frac{E}{2(1+\nu)}$	Shear Modulus	
$\nu = 0.3$	Poisson's ratio	
$\mu = 0.25$	Coefficient of Friction	
N_{Frac}=150	Time steps between fracturing	Floe Fractures
$N_{Pieces} = 3$	Number of pieces for fracturing	
$P_0^* = 5{\times}10^4$ N m^{-1}	Floe strength-to-thickness ratio	
$l_0 = 1$ km	Normalization length scale for size-dependent ice strength	
$\rho_i = 920$ kg m^{-3}	Density of ice	Floe mass and moment of inertia
$\rho_a = 1.2$ kg m^{-3}	Density of air	Surface stresses
$\rho_o = 1027$ kg m^{-3}	Density of ocean	
$Cd_{atm} = 10^{-3}$	Atmosphere-ice drag coefficient	
$Cd_{ocn} = 3{\times}10^{-3}$	Ocean-ice drag coefficient	
$N_{MC} = 100$	Number of sample points for Monte Carlo integration over floe surface	
$\Delta t = 5$ s	Integration time step	Time stepping
$N_b = 25$	Number of floes creating the boundary with islands	Floe state
$N_b = 21$	Number of floes creating the boundary without islands	

2.1.1 Ocean Sensitivity Test

Ocean speeds within the Nares Strait, especially within the Kennedy Channel, are very strong and vary based on season, year, and ice coverage [50]. Since we do not have ocean observations for the considered time period, we perform a sensitivity test to determine the impacts of the underlying ocean currents on model outputs and the appropriate ocean speed for the high-resolution model run with a minimum floe size of one square kilometer. Table 1 presents the model parameters used in the simulation. The wind data from May 10, 2017, to May 20, 2017, are sourced from the AWS on Hans Island, and the ocean is assumed to be pushing in the direction of the channel at velocities of 0.3 m/s and 0.4 m/s [50], moving from the Arctic to Kane Basin. We then use the sea ice area fluxes obtained from the Lincoln Sea flux gate measurements [47] to validate and determine the appropriate ocean velocity. The SubZero code was modified to track the area flux of ice as it passes the flux gate line indicated in Figure 1a. Supplementary Figure 2 in the supplementary material shows the model output sensitivity to the ocean currents on values such as the total area transport. As ocean velocities increase, the area fluxes tend to trend towards higher flux rates, as illustrated in the supplementary figures. The study shows that to match the observed area flux and transport at the one square kilometer resolution, we need to use a surface ocean speed of 0.3 m/s. Existing studies of ocean current observations in the Kennedy Channel using moorings report depth-averaged tidal currents of about 0.2 m/s and multi-year average currents of about 0.05–0.1 m/s [50]. Since sea ice is affected by surface ocean currents

that can typically be much stronger than depth-averaged currents, the inferred estimate of 0.3 m/s may be reasonable.

2.1.2 Resolution Test

We ran multiple resolution tests to determine the model sensitivity to the minimum floe size kept for simulations. The two minimum floe sizes used in this study are 1 km^2 and 10 km^2. The other model parameters used in the simulation are the same as presented in Table 1 from other studies. The winds here are still those from May 10, 2017, to May 20, 2017, and the ocean is assumed to be pushing in the direction of the channel at a velocity of 0.3 m/s based upon the results from section 2.1.1, moving from the Arctic to Kane Basin. Again, we compare this to sea ice area fluxes obtained from the Lincoln Sea flux gate measurements.

The sensitivity experiments show that the size of ice floes can affect the movement of sea ice through narrow straits. As the size of sea ice floes decreases, they can more easily travel through the narrow strait. However, sea ice movement through these straits is not always smooth, as large floes can become jammed in narrow areas (Supplementary Figure 3). This jamming occurs when large floes cluster in narrow parts of the strait, and ice movement can only resume once some of these larger floes break into smaller pieces (Supplementary Figure 4). In the coarser resolution experiments, the floes are more susceptible to jamming, as larger floes can become stuck, while in the experiments with finer resolutions, the floes remain capable of breaking to relieve the stress. The simulated sea ice area fluxes of around 10^3 km^2/day, as well as the distribution of flux rates, compare well to flux-gate observations [20]. However, the coarser simulations tended to underpredict the total amount of ice area transported throughout the run, as illustrated in the Supplementary Figure 3. As the sea ice breaks into smaller floes, they can propagate through the relatively narrow strait. The breaking of floes depends on the fracture criteria, and the floe fractures lead to intermittent but large fluxes of sea ice area and transported mass. The FSD in the model equilibrates to a power-law distribution with an exponent close to -2 for both medium and fine-scale simulations, and compares well to observations over about a decade of floe sizes (Supplementary Figure 3).

2.2 Idealized Test

We use the tuned model to conduct idealized simulations within the Nares Strait, simulating the conditions following the collapse of the southern ice arch. All idealized tests addressing sensitivity to the presence of islands are done with the same initial conditions. Note, however, that these initial conditions are different from the initial conditions in the ocean/resolution tests from Section 2.1.1 and Section 2.1.2. The model simulations have full ice coverage stretching from the Lincoln Sea through the Kennedy Channel, with Kane Basin free of ice. From this setup, we test variations in the ice thickness and the impact of islands.

We evaluate the influence of ice thickness on the simulation by maintaining consistent initial conditions across all test cases, differing only in the thickness of the ice. In the first test, the floes had a uniform thickness of 0.5 meters and covered the northern area of the Kane Basin up to the Lincoln Sea. The second test increased the thickness to 1 meter. The third test featured ice in the strait starting at 1.5 meters thick, while the ice north of the Nares Strait, originating in the Lincoln Sea, began at 2 meters thick. All other parameters are consistent with those listed in Table 1. For all three tests, the minimum floe size was set to one square kilometer, and the ocean speed was maintained at 0 m/s. The wind speeds for these runs were set at 15 m/s, blowing down the channel from the top of the domain to the bottom, with a cross-channel wind speed of 0 m/s. For this study, the model was configured to track the movement of sea ice past the vertical location of Hans Island, situated in the center of the Kennedy Channel. All three scenarios included the islands. We used coastal boundaries and islands, which are designated in the model as indestructible static floes, as was done previously. Supplementary Figure 5 illustrates how ice thickness influences the flux and transport of sea ice through the Nares Strait. Thicker ice exhibits increased resistance to fracturing, leading to more frequent jamming events and a subsequent reduction in ice transport.

We assess the impact of islands on the simulation by utilizing SubZero to simulate runs that start at full sea ice coverage and idealized forcing conditions. To accomplish this, we employ the same initial conditions across all test cases except for the islands within the Kennedy Channel. We ran a suite of tests with and without the islands present within the Kennedy Channel section of Nares Strait over a range of wind speeds to assess the impact of the islands when the channel is completely covered in ice. These floes were of uniform thickness at 0.5 m and covered north of Kane Basin up to the Lincoln Sea. Full ice coverage represents the period when the lower arch is breaking up and the ice is starting to leave the Kennedy Channel. These exact initial floe states were used for all tests. The minimum floe size is one square kilometer, and the ocean speed is set to 0 m/s. For this study, we set the model to track the movement of sea ice past the vertical location of Hans Island in the center of the Kennedy Channel. All other parameters are the same as in table 1. The wind speeds for these runs are 5 m/s, 10 m/s, and 15 m/s, blowing down the channel from the top of the domain, with no winds in the cross-channel direction. We created a set of coastal boundaries and islands that are indestructible static floes, as before; however, for half of the runs, we removed the islands and replaced them with regular floes that can move and break.

2.3 Optical Imagery Observations

To construct an observational estimate of FSD in the Nares Strait, we segmented and retrieved the areas of sea ice floes using optical satellite imagery acquired between May and August over 14 years (2009–2023) for Terra/Aqua satellites at 250 m resolution and 7 years (2016–2023) for Sentinel-2 at 17 m resolution. We selected cloud-free days after the ice breakup within the Nares

Table 2: Comparison of the estimated power-law exponents of the FSDs reconstructed in the Nares Strait from Aqua/Terra (MODIS) and Sentinel-2 satellite imagery obtained on the same days.

Date	Modis	Sentinel-2
2016-07-14	-1.9	-1.7
2019-06-08	-2.8	-2.8
2019-07-25	-1.8	-2
2022-05-13	-2.3	-1.75
2022-06-15	-2.5	-2.6
2022-07-25	-2.3	-2.5
2023-07-14	-2.2	-2.2

Strait to ensure individual ice fragments could be identified. The images used have been made publicly available (see data availability) with image dates indicated in the file names. Floe identification was achieved through an image segmentation algorithm [51], which utilizes a modified "restricted growing" approach [33, 52]. The image was preprocessed into a binary image and manually classified into ice (floes) and water (background) based on a grayscale threshold, followed by an iterative erosion-expansion scheme to produce a segmented image. Any floes cut off by the image borders or located on land were removed.

The segmented images are utilized to construct an FSD [12] that we have defined in the following way. We use the cumulative FSD form, $FSD(x)$, defined as the fractional number of floes with sizes larger than size x, where the floe size is defined for simplicity as the square root of its area. Unlike in previous studies, we normalized FSD by the total area of the identified floes rather than the image's total area. This adjustment ensures consistency in the FSD definition by accounting for changes in the land mask and sea ice concentration between different images. The observed FSD can be characterized by a single power law with an exponent alpha computed using a slope of linear least-squares fit in the log-log space for the range of floe sizes covered by lower-resolution Terra/Aqua imagery. The power law exponent values are compared with the higher-resolution Sentinel-2 in Table 2.

3 Results

For model-data comparison, we reconstructed an FSD from segmenting floes from satellite images in the Nares Strait (see Section 3.1) and used sea ice area fluxes obtained from existing Lincoln Sea flux gate measurements [47] at the entrance of the Nares Strait. In Section 3.2, we use the observations to demonstrate the model's adequacy in simulating the observed statistics of sea ice motion. In Section 3.3, we quantify the role of the islands by comparing sea ice dynamics in simulations that include or exclude the islands.

3.1 Observations of Transport and FSD in Nares Strait

Sea ice area transport through Nares Strait exhibits highly intermittent behavior, with some events being nearly three times stronger than its average

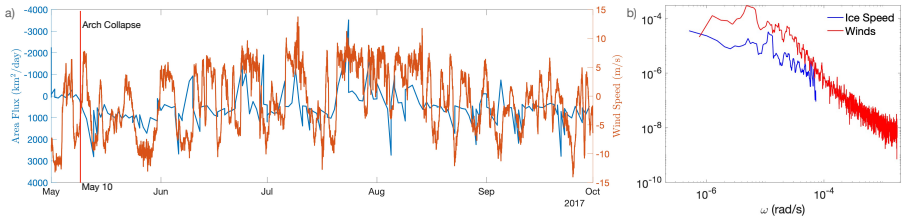

Fig. 2: Observations of winds and sea ice area fluxes in the Nares Strait. a) Observational sea ice area flux and wind speed aligned with the channel that forces the ice from May through Sept 2017 (Data taken from the atmospheric station on Hans Island and the southern Lincoln Sea flux gate). The observational area flux is positive when moving from the Lincoln Sea into the Nares Strait. The wind speed plotted here is aligned with the channel and is negative when moving in the direction from top to bottom. The simulation time used to force the model for this study is May 10 to May 20, 2017). b) The power spectral density of the observed ice and along-channel wind velocities from 2017 dates shown in (a). The power spectrum for winds is scaled by a factor of 0.02, which demonstrates where the ice velocity would be if it were roughly in free drift. The gap in the power spectrum shows that energy is lost to ice-ice and ice-land interactions.

transport and other times having almost no transport (Figure 2a). Right after an arch collapse (an example is shown for May 10, 2017, for which flux gate observations exist), there is a rapid transport of ice that is driven by strong southward winds, with an average sea ice transport of about 1000 km^2 per day over the course of the summer. However, the sea ice motion is not in free drift, as is clearly indicated by the discrepancy in the power spectra of the observed sea ice velocities and expected free-drift velocity based on the wind speeds, particularly at time scales longer than about a day (Figure 2b). Sea ice moving significantly slower than expected in free drift indicates that it looses energy and momentum not only due to ocean drag but also due to internal collisions and interactions with coastlines. The intermittency of sea ice transport is associated with a combination of strongly varying atmospheric winds and granular behavior of sea ice floes that leads to jamming. Note that for simulation purposes, we use the local Hans Island winds because they capture extreme wind events that are absent in the reanalysis data [45, 46].

Since there are no existing comprehensive observational studies on FSD in the Nares Strait, we developed a database of cloud-free optical images of sea ice taken from two satellites with very different resolutions (Terra at 250 m resolution and Sentinel-2 at 17 m). The sea ice images span the post-arch collapse period (from May to August) over a 14-year period (2009–2023) for Terra and a seven-year period (2016–2023) for Sentinel-2. The individual ice floes and their sizes were identified via the image segmentation algorithm [51]

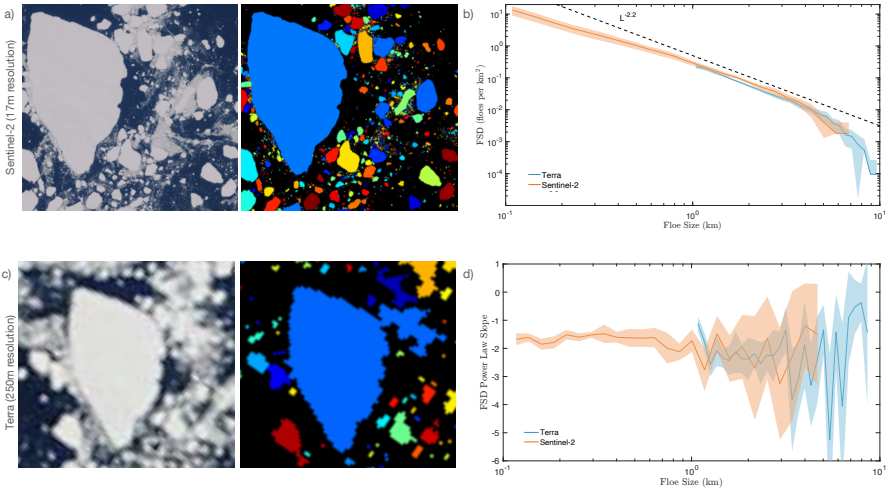

Fig. 3: The segmentation process of sea ice floes from the Aqua/Terra satellite reflectance images at 250 m resolution and Sentinel-2 at 17 m resolution. a) Input image and resulting segmented image from Sentinel-2. Image taken from SentinelHub for 2022-06-16 b)The FSDs for both the Aqua/Terra and Sentinel-2 satellites. c) Input image and resulting segmented image from Terra. Image taken from NASA Worldview for 2022-06-16. d) The power-law slope fit comparing Terra and higher resolution Sentinel-2. The shadings in parts (b) and (d) indicate the 95% confidence intervals.

(see Figure 3 and Methods 2). FSDs estimated from both satellites are remarkably similar, following an approximate power-law distribution for a wide range of floe sizes (Figure 3b). The values of the best-fit power-law exponent range from about -1.7 to -2.8, with a mean of -2.2 across all images. This range of power laws falls within the range of existing FSD observations in other regions of the Arctic Ocean [28]. Note that here we present FSD as a function of floe size defined as the square root of its area; for the FSD expressed in terms of floe area, the mean power-law exponent of -2.2 would translate to $\frac{1}{2}(-2.2) - 1 = -2.1$. Comparing it to the recent area-based FSD power-law estimate of [-2,-1.65] obtained using segmentation of very high-resolution (about 1 m) MEDEA images in the Canada Basin [33], there is also a good agreement. This suggests that floe fracturing processes in Nares Strait might be representative of many other regions of the Arctic Ocean.

3.2 Granular simulations of sea ice flow in Nares Strait

We conducted a process study to tune the model to the observational statistics from the Nares Strait described in section 3.1. We initialized the model with an ice concentration taken from post-collapse observations of a northern ice arch (Figure 4a) and forced the model with observed winds and prescribed

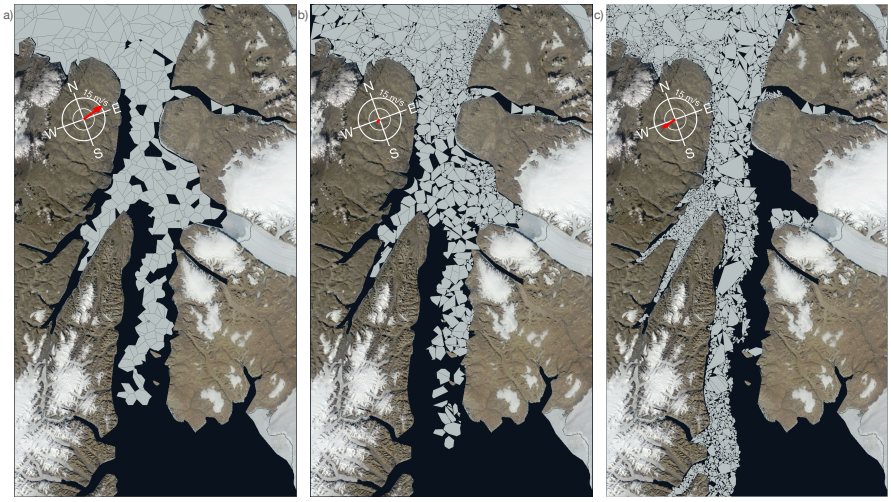

Fig. 4: The SubZero simulation showing the evolution of sea ice floes as they propagate through Nares Strait. The three panels show the progression of the modeled state of ice floes as they evolve from a) unrealistic initial conditions where all floes have similar sizes to b) the state 1.5 days into the simulation after the winds have caused collisions and fractures that are particularly evident in the northern part of the channel, and c) the state 10 days into the simulation when the distribution of floe sizes have reached statistical equilibrium. The simulation resolves collisions of floes down to the minimum size of 1 km^2 and uses the scale-dependent fracture criteria (see Methods).

ocean currents as described in methods. (See section 2). The sea ice evolves from unrealistic initial conditions, with primarily uniform floe sizes, to a state with a wide range of floe sizes due to cascading floe fractures (Figure 4). During model tuning, nearly all model parameters remained the same as in the default model configuration [43] (see Table 1). However, we identified two key processes that most significantly impacted the sea ice statistics. Those two processes are the strength of ocean currents, which mainly affect the mean sea ice transport, and the parameterization of the floe strength for floe fractures, which mainly affect the FSD. Since there are no ocean observations coincident with flux gate and wind observations, we assumed a highly idealized ocean with constant currents moving down the channel. The ocean currents provide additional forcing to the sea ice and mainly affect the mean value of the sea ice area transport (see section 2.1.1). However, ocean currents did not impact the emerging power-law exponent of the FSD. To better match the model FSD to observations, we incorporated a scale-dependent parameterization for the floe strength ($P^* \sim l^{-\frac{1}{2}}$) that was previously proposed in an observational study of sea ice fractures [11]. This parameterization assumes the floe strength, P^*, to be inversely proportional to the square root of its length scale, l, implying that larger floes could fracture under less stress (see Methods).

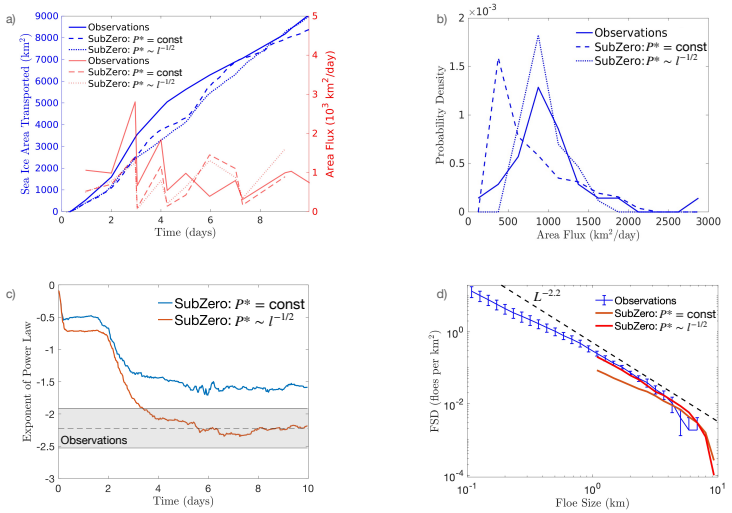

Fig. 5: The observed and modeled characteristics of sea ice floes and transport. a) The cumulative area transport for the SubZero simulation for scale-independent ($P^* = const$) and scale-dependent ($P^* \sim l^{-\frac{1}{2}}$) floe strength, compared to the observed area transport and the instantaneous fluxes over the 10-day simulation period. b) The associated probability density function (PDF) for the fluxes with the two runs compared to observations of fluxes for the month following the collapse of the sea ice arch. c) Shows the time evolution of the instantaneous exponent of the power law over the run for a run with size-dependent fracture laws and one with size-independent fracture laws. d) The mean FSD for days four through 10 for size-dependent fracture laws, size-independent fracture laws, and the mean observed FSD from the Nares Strait from Sentinel-2 imagery.

Upon only adjusting the strength of ocean currents and the floe fracture parameterization, quantitative metrics including FSD, mean transport, and the probability distribution of sea ice area fluxes, reasonably agree with flux-gate observations during the May 2017 period [20] and the satellite-derived FSD (Figure 5). The sea ice area fluxes measured in Nares Strait from flux-gate observations are on the order of $O(10^3)$ km^2/day [20]. The total integrated ice area transport, which represents the cumulative amount of ice that has moved past the island during the simulation period, generally aligns with the simulation results (Figure 5a). Both the total integrated amount of ice transport over the simulation period and the instantaneous ice fluxes closely mirrored the observed patterns. A comparison of the observed distribution of the area fluxes over the breakup month (May 2017) to the modeled one also shows a good agreement (Figure 5b). Simulated mean area fluxes are around 1000 km^2/day, and the distribution has fat tails, with less frequent events having either very small transports or nearly triple the mean, which is similar to observations [14, 20].

The intermittency of area fluxes reflects the presence of floe jamming events, followed by spontaneous breakup and rapid sea ice motion (see Supplementary Video 1). As sea ice collisions lead to fracture events that generate smaller and smaller floes, these floes can then propagate through the relatively narrow strait. After about five days of spin-up time, the modeled FSD equilibrates to a power-law distribution with a best-fit exponent that is about -1.5 for the case of scale-independent and -2.2 for the scale-dependent floe strength (Figure 5c). Comparing the modeled and satellite-derived FSDs, we find a remarkable agreement for simulations with scale-dependent floe strength (Figure 5d). Using the scale-dependent criteria also leads to the distribution of area fluxes that is much more consistent with observations (Figure 5b), confirming a connection between the statistics of floe jamming/breakup events and FSD. Our simulations thus imply that larger floes are relatively weaker compared to smaller floes, with the floe strength required for a floe to fracture scaling inversely with the square root of the floe size. Since the SubZero model can reasonably reproduce the crucial observational characteristics of sea ice floes, including the power-law FSD, intermittency of area fluxes, and overall transport, we proceed to quantify the role of the islands in sea ice transport.

3.3 Impact of islands on sea ice motion

To evaluate the influence of islands on ice transport, we use the tuned model to conduct two types of simulations, with and without islands, and explore the response of sea ice to external forcing that we vary by using uniform winds of different strengths. At the start of both cases, with and without islands, the size of sea ice floes decreases through fracturing so they can more easily travel through the narrow strait (Supplementary Video 2). However, sea ice movement through these straits is only sometimes smooth, as large floes can become jammed in narrow areas, especially when islands are present. During a typical jamming event (Figure 6a), sea ice velocities near Hans Island are slowed to virtually zero, and the ice can not get past the island until stresses in that area build to the point of fracturing the ice floes. This jamming occurs when large floes cluster in narrow parts of the strait, and ice movement can only resume once some of these larger floes break into smaller pieces. However, when the islands are removed, it becomes much more challenging for the ice floes to jam, and sea ice moves relatively smoothly (Figure 6b). Due to the island-induced jamming events, the average sea ice area flux through the strait is dramatically reduced, particularly in simulations with relatively low wind speeds (Figure 7). In this section, the ice fluxes are calculated as they pass Hans Island. Excluding islands from the simulation nearly doubles the mean area flux and substantially reduces its variance because jamming becomes virtually negligible (see the lack of events with very weak area fluxes in Figure 7a). As the external wind forcing increases, floe fractures become more frequent, reducing the potential for jamming to occur and making the mean sea ice transport in the simulations with and without the islands more similar (Figure 7b).

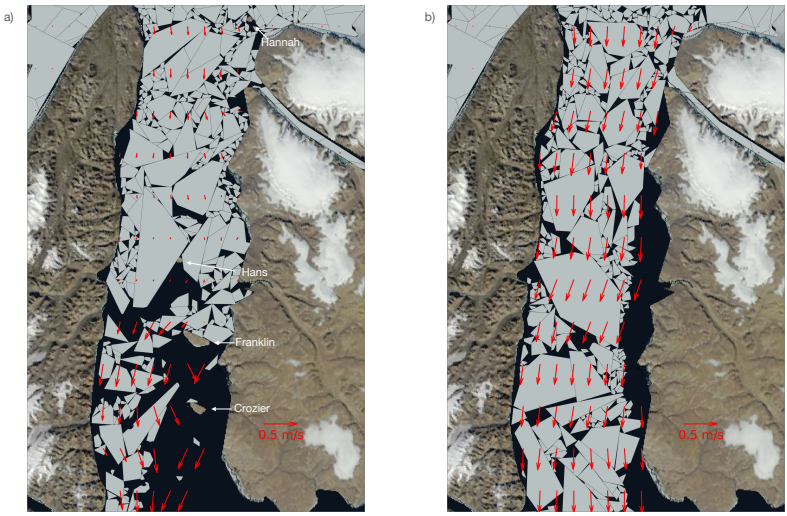

Fig. 6: SubZero simulation snapshots showing the state of sea ice floes as they propagate through Nares Strait with and without islands. This figure compares simulations with a minimum floe size of 1 km^2 and floe size-dependent fractures for runs with and without the islands present. Wind speeds are constant at 10 m/s, blowing from top to bottom. The arrows show equispaced spatially averaged instantaneous ice velocities. a) A snapshot of the model state five days into the run with islands. b) A snapshot of the model state five days into the run without islands.

During jamming events, when the ice gets pinned near islands and barely moves, forces from the ice colliding with the islands and other coastal boundaries oppose the internal stress gradients that build up from local and remote atmospheric forcing. By domain-averaging collision and surface forces experienced by individual floes computed from model output, we identified the contributions of the individual islands and other coastal boundaries to the momentum balance (Figure 8). Note that the magnitudes of the forces from Hans Island in Figure 8 are consistent with forces observationally measured during ice collisions with Hans Island and structures [24, 53, 54]. During a major jamming event around day five (distribution of sea ice floes during this event is shown in Figure 6a), there is a clear spike in the collision forces from Hans Island exerted on the ice, accompanied by a drop in the sea ice area flux (Figure 8a). There are many similar jamming events that do not lead to a complete blockage of sea ice but rather a substantial reduction in transport: for example, on Day 4, when Hans Island plays a big role, or close to Day 10, when Franklin Island is a key contributor to the partial jamming (Figure 8a).

During jamming, there is weak ocean drag as sea ice velocity is low, and the ocean currents are set to zero in these simulations. As such, forces from islands/coasts oppose the external atmospheric forcing during jamming events. Considering the time-average breakdown of the momentum budget in the

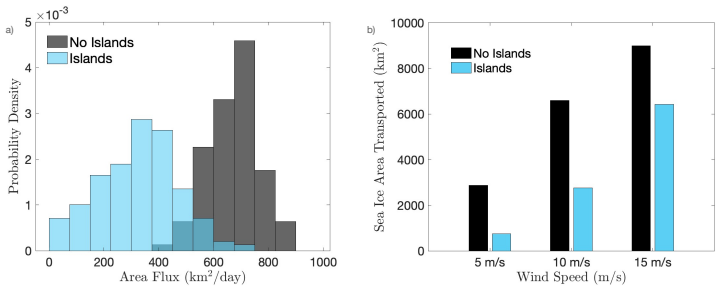

Fig. 7: The sea ice area fluxes and transport in Nares Strait from numerical simulations with and without islands. a) The distribution of sea ice area fluxes for the simulation using 10 m/s winds, with and without islands. b) The sea ice area transported over the total duration of the model simulation (about 10 days), computed at the channel location near Hans Island, and plotted for different wind speeds. Note that direct comparisons of the fluxes with the tuning simulation that used realistic winds and optimized ocean currents (Figure 3.2) would lead to fluxes being biased low because the ocean in the sensitivity experiments shown here is taken to be stationary.

simulation with islands, combined forces from islands and coastlines become dominant, while the ocean drag provides a substantially smaller contribution because of the reduced sea ice velocity compared to the simulation without the islands (Figure 8b). The islands not only provide direct collision forces but also lead to increased frictional forces at lateral coastal boundaries because the ice is pushed toward the channel's lateral boundaries as it propagates around the islands. Thus, the substantial weakening of sea ice transport when islands are included in simulations is due to the combined effect of having normal forces from ice floe collisions with islands and increased frictional forces at the coastal boundaries.

4 Discussion

This investigation emphasizes the important role of small islands in sea ice transport through the Nares Strait after the collapse of sea ice arches. Using a novel floe-scale sea ice model, SubZero, we conducted a process study to explain the observed characteristics of summer sea ice floes as they progressively break up due to collisions with each other and coastal boundaries (see Section 3.3). Such conditions, where new ice is not being formed and floes do not weld but predominantly fracture due to collisions, provided a natural laboratory to focus on the granular aspects of sea ice dynamics. We demonstrated that the model is capable of emulating the jamming and fracturing of floes and the associated wide-tail distribution of sea ice area transport following the breakup of the sea ice arches. Accurately capturing the observed FSD in the

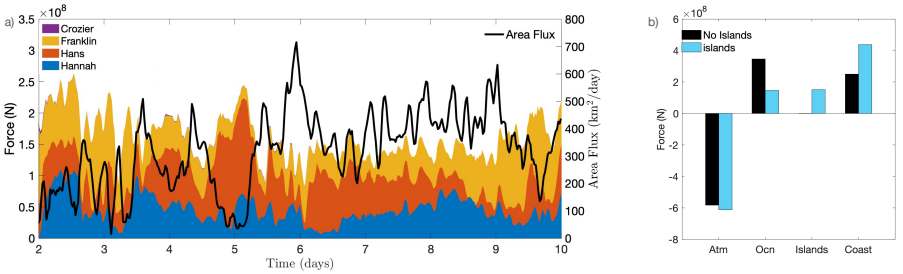

Fig. 8: Domain-averaging collision and surface forces breakdown. (a) The left y-axis shows the combined forces from islands over the final eight days of simulation, comparing with and without islands after a two-day spin-up for 10 m/s winds. The upper boundary displays the total force of the islands at each instant, with colors indicating the portion from each individual island. The right y-axis measures the evolution of the sea ice area flux past Hans Island in Nares Strait over the final eight days of simulation with islands. (b) The time-average breakdown of the y-momentum budget for the 10 m/s winds simulations with and without islands. Mean values are taken over the last eight days of the run.

model requires larger floes fracturing subject to lower stresses, following a size-dependent power-law distribution where the floe strength scales inversely with the square root of the floe size. Compared to using a constant floe strength for all floes, the scale-dependent floe strength leads to FSD with a steeper slope and a significantly higher number of smaller ice floes. This change in FSD impacts intermittent jamming through a slight decrease in jamming events, evidenced by the reduced presence of fat tails in the distribution. However, it is important to note that the FSD has a diminished impact on average transport in our scenario simulations.

By simplifying the model down to only collision-induced fractures and being able to reproduce the major aspects of the observed sea ice behavior, we demonstrated the significance of the granular-type sea ice dynamics. As sea ice floes propagate through the channel, the islands act as anchor points, causing frequent jamming events that significantly reduce long-term sea ice transport, especially during low to moderate wind conditions. In addition to intermittent jamming, the islands cause the coastal drag to increase by pushing the ice toward lateral coastal boundaries. This process study demonstrates the effectiveness of floe-scale modeling in accurately simulating sea ice dynamics in regions with islands and complex coastlines. The omission of islands, typical in climate models, could lead to significant overestimation of sea ice transport from the Arctic through the Nares Strait, contributing to uncertainties in predicting sea ice in our evolving climate.

While our study focused on sea ice propagation after an arch collapse, understanding the formation of sea ice arches (or bridges) is also important because it leads to a total shutdown of ice export through Nares Strait. Frequent jamming events caused by the presence of islands may facilitate arch formation if they coincide with sufficiently low atmospheric temperatures to create new ice and weld existing floes together. It is necessary for climate models to accurately represent processes leading to the formation and collapse of arches, especially as the observed frequency of arch formation is changing with climate. Since climate models are typically too coarse to include small islands, it may be possible to use them in conjunction with regional floe-scale models such as SubZero to represent the effects of islands and complex coastal features in important regions like the Nares Strait. Another way to improve continuous sea ice models used in climate simulations is to develop parameterizations based on floe-scale models. Finally, we emphasize the need for high-resolution sea ice observations to improve and fine-tune floe-scale models to better understand the granular nature of sea ice.

5 Conclusion

In this study, we investigated the dynamics of sea ice within Nares Strait, utilizing the floe-scale model, SubZero, to elucidate the impact of small islands on ice transport mechanisms. Our findings reveal that these islands play a crucial role in altering sea ice movement by creating localized blockages that can impede flow. The presence of islands leads to increased collision forces between ice and the land, resulting in significant floe fragmentation and a complex interplay of interactions that are critical for understanding the transport dynamics in this region. Through simulations that incorporated both the presence and absence of islands, we show that islands significantly reduce the sea ice transport. We demonstrated that a size-dependent floe strength criterion is essential for accurately capturing the observed floe size distribution and its power-law behavior. The study highlights the nuances of sea ice behavior, illustrating how interactions with islands can shape the overall ice landscape. Furthermore, we emphasize the importance of floe-scale models to gain a deeper understanding of the intricate characteristics of sea ice's granular nature. While the SubZero model effectively captured these dynamics, it also revealed areas for further enhancement to improve its operational applicability. Future efforts will focus on refining the model to better simulate the diverse processes involved in floe interactions and assessing its response under varying climatic scenarios. This research not only enhances our understanding of the intricate sea ice dynamics within Nares Strait but also emphasizes the importance of considering localized physical features, such as small islands, in broader climate modeling efforts. These insights are vital for accurately predicting the consequences of climate change on Arctic sea ice behavior and its implications for the global climate system.

Open Research Section

The most up to date SubZero code [55] is provided at the public GitHub repository https://github.com/SeaIce-Math/SubZero. SubZero v1.0.5 [56] associated with this publication and test cases shown above can be found on Zenodo https://doi.org/10.5281/zenodo.17392675. The images used for observational FSD calculations can be found on Zenodohttps://doi.org/10.5281/zenodo.13770011. The author would like to thank the Scottish Association for Marine Sciences for access to the Hans Island automatic weather station data (https://dataservices.sams.ac.uk/aws/).

Acknowledgments

B.P.M and G.E.M gratefully acknowledge support from the Office of Naval Research (ONR) grant N00014-19-1-2421 and the National Science Foundation CAREER Award No. 2338233. The authors are extremely grateful for the valuable contributions made by our undergraduate researchers, Yuna Liu and Camille Viviani, to this research. The authors also highly appreciate the insightful discussions at the online workshop "Modeling the Granular Nature of Sea Ice" organized by the School of Oceanography, University of Washington as part of the ONR MURI project N00014-19-1-2421. The manuscript benefited greatly from the reviews provided by the reviewers.

References

[1] Chiang, J.C., Bitz, C.M.: Influence of high latitude ice cover on the marine intertropical convergence zone. *Climate Dynamics* **25**(5), 477–496 (2005). https://doi.org/10.1007/s00382-005-0040-5

[2] Curry, J.A., Schramm, J.L., Ebert, E.E.: Sea ice-albedo climate feedback mechanism. *Journal of Climate* **8**(2), 240–247 (1995). https://doi.org/10.1175/1520-0442(1995)008⟨0240:SIACFM⟩2.0.CO;2

[3] Deser, C., Walsh, J.E., Timlin, M.S.: Arctic sea ice variability in the context of recent atmospheric circulation trends. *Journal of Climate* **13**(3), 617–633 (2000). https://doi.org/10.1175/1520-0442(2000)013⟨0617:ASIVIT⟩2.0.CO;2

[4] Ding, Q., Schweiger, A., L'Heureux, M., Steig, E.J., Battisti, D.S., Johnson, N.C., Blanchard-Wrigglesworth, E., Po-Chedley, S., Zhang, Q., Harnos, K., et al.: Fingerprints of internal drivers of arctic sea ice loss in observations and model simulations. Nature Geoscience **12**(1), 28–33 (2019). https://doi.org/10.1038/s41561-018-0256-8

[5] Spreen, G., de Steur, L., Divine, D., Gerland, S., Hansen, E., Kwok, R.: Arctic sea ice volume export through fram strait from 1992 to 2014.

Journal of Geophysical Research: Oceans **125**(6), 2019–016039 (2020). https://doi.org/10.1038/s43247-024-01296-9

[6] Babb, D.G., Galley, R.J., Howell, S.E., Landy, J.C., Stroeve, J.C., Barber, D.G.: Increasing multiyear sea ice loss in the beaufort sea: A new export pathway for the diminishing multiyear ice cover of the arctic ocean. *Geophysical Research Letters* **49**(9), 2021–097595 (2022). https://doi.org/10.1029/2021GL097595

[7] Howell, S., Babb, D., Landy, J., Moore, G., Montpetit, B., Brady, M.: A comparison of arctic ocean sea ice export between nares strait and the canadian arctic archipelago. *Journal of Geophysical Research: Oceans* **128**(4), 2023–019687 (2023). https://doi.org/10.1029/2023JC019687

[8] Zhang, J., Weijer, W., Steele, M., Cheng, W., Verma, T., Veneziani, M.: Labrador sea freshening linked to beaufort gyre freshwater release. *Nature communications* **12**(1), 1229 (2021). https://doi.org/10.1038/s41467-021-21470-3

[9] Yashayaev, I.: Intensification and shutdown of deep convection in the labrador sea were caused by changes in atmospheric and freshwater dynamics. *Communications Earth & Environment* **5**(1), 156 (2024)

[10] Weiss, J.: Fracture and fragmentation of ice: a fractal analysis of scale invariance. *Engineering Fracture Mechanics* **68**(17-18), 1975–2012 (2001). https://doi.org/10.1016/S0013-7944(01)00034-0

[11] Weiss, J., Schulson, E.M.: Coulombic faulting from the grain scale to the geophysical scale: lessons from ice. *Journal of Physics D: Applied Physics* **42**(21), 214017 (2009). https://doi.org/10.1088/0022-3727/42/21/214017

[12] Rothrock, D.A., Thorndike, A.S.: Measuring the sea ice floe size distribution. *Journal of Geophysical Research: Oceans* **89**(C4), 6477–6486 (1984). https://doi.org/10.1029/JC089iC04p06477

[13] Damsgaard, A., Adcroft, A., Sergienko, O.: Application of discrete element methods to approximate sea ice dynamics. *Journal of Advances in Modeling Earth Systems* **10**(9), 2228–2244 (2018). https://doi.org/10.1029/2018MS001299

[14] Kwok, R., Toudal Pedersen, L., Gudmandsen, P., Pang, S.: Large sea ice outflow into the nares strait in 2007. *Geophysical Research Letters* **37**(3) (2010). https://doi.org/10.1029/2009GL041872

[15] Rallabandi, B., Zheng, Z., Winton, M., Stone, H.A.: Formation of sea ice bridges in narrow straits in response to wind and water stresses. *Journal*

of Geophysical Research: Oceans **122**(7), 5588–5610 (2017). https://doi.org/10.1002/2017JC012822

[16] Rallabandi, B., Zheng, Z., Winton, M., Stone, H.A.: Wind-driven formation of ice bridges in straits. *Physical review letters* **118**(12), 128701 (2017). https://doi.org/10.1103/PhysRevLett.118.128701

[17] Moore, G., Howell, S., Ballinger, T., McNeil, K., Brady, M.: Contribution of ice dynamics along nares strait to the stability of ice arches. Preprint at https://doi.org/10.21203/rs.3.rs-3976407/v1 (2024)

[18] Kirillov, S., Babb, D., Komarov, A., Dmitrenko, I., Ehn, J., Worden, E., Candlish, L., Rysgaard, S., Barber, D.: On the physical settings of ice bridge formation in nares strait. *Journal of Geophysical Research: Oceans* **126**(8), 2021–017331 (2021). https://doi.org/10.1029/2021JC017331

[19] Moore, G., Howell, S., Brady, M.: Evolving relationship of nares strait ice arches on sea ice along the strait and the north water, the arctic's most productive polynya. *Scientific Reports* **13**(1), 9809 (2023). https://doi.org/10.1038/s41598-023-36179-0

[20] Moore, G., Howell, S., Brady, M., Xu, X., McNeil, K.: Anomalous collapses of nares strait ice arches leads to enhanced export of arctic sea ice. *Nature communications* **12**(1), 1 (2021). https://doi.org/10.1038/s41467-020-20314-w

[21] Detlef, H., Reilly, B., Jennings, A., Mørk Jensen, M., O'Regan, M., Glasius, M., Olsen, J., Jakobsson, M., Pearce, C.: Holocene sea-ice dynamics in petermann fjord in relation to ice tongue stability and nares strait ice arch formation. *The Cryosphere* **15**(9), 4357–4380 (2021). https://doi.org/10.5194/tc-15-4357-2021

[22] Detlef, H., O'Regan, M., Stranne, C., Jensen, M.M., Glasius, M., Cronin, T.M., Jakobsson, M., Pearce, C.: Seasonal sea-ice in the arctic's last ice area during the early holocene. Communications Earth & Environment **4**(1), 86 (2023). https://doi.org/10.1038/s43247-023-00720-w

[23] Joshy, K., Moore, G., McNeil, K.: Transient wind-driven polynyas within nares strait. Preprint at 10.22541/essoar.171501009.93805419/v1 (2024)

[24] Danielewicz, B., Metge, M., Dunwoody, A.: On estimating large scale ice forces from deceleration of ice floes. *The Seventh International Conference on Port and Ocean Engineering under Arctic Conditions*, 537–546 (1983)

[25] Nimmo, R.: Ice Monitoring During Arctic Petroleum Exploration. http://nauticapedia.ca/Gallery/Arctic_Ice_Monitoring.php. Nauticapedia.ca, 2017 (2017)

[26] Cates, M., Wittmer, J., Bouchaud, J.-P., Claudin, P.: Jamming, force chains, and fragile matter. *Physical review letters* **81**(9), 1841 (1998). https://doi.org/10.1103/PhysRevLett.81.1841

[27] To, K., Lai, P.-Y., Pak, H.: Jamming of granular flow in a two-dimensional hopper. *Physical review letters* **86**(1), 71 (2001). https://doi.org/10.1103/PhysRevLett.86.71

[28] Stern, H.L., Schweiger, A.J., Zhang, J., Steele, M.: On reconciling disparate studies of the sea-ice floe size distribution. *Elem Sci Anth* **6**, 49 (2018). https://doi.org/10.1525/elementa.304

[29] Stern, H.L., Schweiger, A.J., Stark, M., Zhang, J., Steele, M., Hwang, B.: Seasonal evolution of the sea-ice floe size distribution in the beaufort and chukchi seas. *Elem Sci Anth* **6**, 48 (2018). https://doi.org/10.1525/elementa.305

[30] Hwang, B., Wilkinson, J., Maksym, T., Graber, H.C., Schweiger, A., Horvat, C., Perovich, D.K., Arntsen, A.E., Stanton, T.P., Ren, J., Wadhams, P.: Winter-to-summer transition of arctic sea ice breakup and floe size distribution in the beaufort sea. *Elem Sci Anth* **5**, 40 (2017). https://doi.org/10.1525/elementa.232

[31] Horvat, C.: Floes, the marginal ice zone and coupled wave-sea-ice feedbacks. *Philosophical Transactions of the Royal Society A* **380**(2235), 20210252 (2022). https://doi.org/10.1098/rsta.2021.0252

[32] Zhang, Q., Hughes, N.: Ice floe segmentation and floe size distribution in airborne and high-resolution optical satellite images: towards an automated labelling deep learning approach. *The Cryosphere* **17**(12), 5519–5537 (2023)

[33] Denton, A.A., Timmermans, M.-L.: Characterizing the sea-ice floe size distribution in the canada basin from high-resolution optical satellite imagery. *The Cryosphere* **16**(5), 1563–1578 (2022). https://doi.org/10.5194/tc-16-1563-2022

[34] Buckley, E.M., Cañuelas, L., Timmermans, M.-L., Wilhelmus, M.M.: Seasonal evolution of the sea ice floe size distribution in the beaufort sea from 2 decades of modis data. The Cryosphere **18**(11), 5031–5043 (2024). https://doi.org/10.5194/tc-17-5519-2023

[35] Keen, A., Blockley, E., Bailey, D.A., Boldingh Debernard, J., Bushuk, M., Delhaye, S., Docquier, D., Feltham, D., Massonnet, F., O'Farrell, S., Ponsoni, L., Rodriguez, J.M., Schroeder, D., Swart, N., Toyoda, T., Tsujino, H., Vancoppenolle, M., Wyser, K.: An inter-comparison of the mass budget of the arctic sea ice in cmip6 models. *The Cryosphere* **15**(2),

951–982 (2021). https://doi.org/10.5194/tc-15-951-2021

[36] Hunke, E.C., Dukowicz, J.K.: An elastic–viscous–plastic model for sea ice dynamics. *Journal of physical oceanography* **27**(9), 1849–1867 (1997). https://doi.org/10.1175/1520-0485(1997)027⟨1849:AEVPMF⟩2.0.CO;2

[37] Dansereau, V., Weiss, J., Saramito, P., Lattes, P., Coche, E.: Ice bridges and ridges in the maxwell-eb sea ice rheology. *The Cryosphere* **11**(5), 2033–2058 (2017). https://doi.org/10.5194/tc-11-2033-2017

[38] Rasmussen, T.A., Kliem, N., Kaas, E.: Modelling the sea ice in the nares strait. *Ocean Modelling* **35**(3), 161–172 (2010). https://doi.org/10.1016/j.ocemod.2010.07.003

[39] Hopkins, M.A.: A discrete element lagrangian sea ice model. Engineering Computations **21**(2/3/4), 409–421 (2004). https://doi.org/10.1108/02644400410519857

[40] Hopkins, M.A., Thorndike, A.S.: Floe formation in arctic sea ice. Journal of Geophysical Research: Oceans **111**(C11) (2006). https://doi.org/10.1029/2005JC003352

[41] Åström, J., Robertsen, F., Haapala, J., Polojärvi, A., Uiboupin, R., Maljutenko, I.: A large-scale high-resolution numerical model for sea-ice fragmentation dynamics. *The Cryosphere* **18**(5), 2429–2442 (2024). https://doi.org/10.5194/tc-18-2429-2024

[42] West, B., O'Connor, D., Parno, M., Krackow, M., Polashenski, C.: Bonded discrete element simulations of sea ice with non-local failure: Applications to nares strait. *Journal of Advances in Modeling Earth Systems* **14**(6), 2021–002614 (2022). https://doi.org/10.1029/2021MS002614

[43] Manucharyan, G.E., Montemuro, B.P.: Subzero: A sea ice model with an explicit representation of the floe life cycle. *Journal of Advances in Modeling Earth Systems*, 2022–003247 (2022). https://doi.org/10.1029/2022MS003247

[44] Montemuro, B.P., Manucharyan, G.E.: Subzero: a discrete element sea ice model that simulates floes as evolving concave polygons. *Journal of Open Source Software* **8**(88), 5039 (2023). https://doi.org/10.21105/joss.05039

[45] Moore, G.: Impact of model resolution on the representation of the wind field along nares strait. *Scientific Reports* **11**(1), 13271 (2021). https://doi.org/10.1038/s41598-021-92813-9

[46] Moore, G., Imrit, A.: Impact of resolution on the representation of the mean and extreme winds along nares strait. *Journal of Geophysical*

Research: Atmospheres **127**(19), 2022–037443 (2022). https://doi.org/10.1029/2022JD037443

[47] Moore, G.: Nares Strait Ice Area Flux. Borealis (2019). https://doi.org/10.5683/SP2/WRGX0K. https://doi.org/10.5683/SP2/WRGX0K

[48] Åström, J.: Statistical models of brittle fragmentation. Advances in Physics **55**(3-4), 247–278 (2006). https://doi.org/10.1080/00018730600731907

[49] Hibler, W.D.: A dynamic thermodynamic sea ice model. *Journal of physical oceanography* **9**(4), 815–846 (1979). https://doi.org/10.1175/1520-0485(1979)009⟨0815:ADTSIM⟩2.0.CO;2

[50] Münchow, A.: Volume and freshwater flux observations from nares strait to the west of greenland at daily time scales from 2003 to 2009. Journal of Physical Oceanography **46**(1), 141–157 (2016). https://doi.org/10.1175/JPO-D-15-0093.1

[51] Denton, A.A.: Sea-Ice Floe Segmentation. Zenodo (2022). https://doi.org/10.5281/zenodo.6336109

[52] Soh, L.-K., Tsatsoulis, C., Holt, B.: Identifying ice floes and computing ice floe distributions in SAR images, pp. 9–34. Springer, ??? (1998). https://doi.org/10.1007/978-3-642-60282-5_2

[53] Masterson, D., Frederking, R.: Local contact pressures in ship/ice and structure/ice interactions. Cold Regions Science and Technology **21**(2), 169–185 (1993). https://doi.org/10.1016/0165-232X(93)90005-S

[54] Timco, G.W., Frederking, R.M.W.: Overview of Historical Canadian Beaufort Sea Information. Canadian Hydraulics Centre, National Research Council of Canada, ??? (2008). https://doi.org/10.4224/20178991

[55] Manucharyan, G.E., Montemuro, B.P.: SubZero sea ice model. GitHub (2022)

[56] Montemuro, B.P., Manucharyan, G.E.: SubZero: a discrete element sea ice model that simulates floes as evolving concave polygons. Zenodo (2024). https://doi.org/10.5281/zenodo.13730444